Batteries & Supercaps

Research Article
doi.org/10.1002/batt.202200565

Chemistry Europe
European Chemical Societies Publishing

www.batteries-supercaps.org

Understanding the Electrochemical and Interfacial Behavior of Sulfolane based Electrolyte in $LiNi_{0.5}Mn_{1.5}O_4$-Graphite Full-Cells

Girish D. Salian,[a] Alma Mathew,[a] Ritambhara Gond,[a] Wessel van Ekeren,[a] Jonathan Højberg,[b] Christian Fink Elkjær,[b] Matthew J. Lacey,[c] Satu Kristiina Heiskanen,[d] Daniel Brandell,[a] and Reza Younesi*[a]

An ethylene carbonate-free electrolyte composed of 1 M lithium bis(fluorosulfonyl) imide (LiFSI) in sulfolane (SL) is studied here for $LiNi_{0.5}Mn_{1.5}O_4$-graphite full-cells. An important focus on the evaluation of the anodic stability of the SL electrolyte and the passivation layers formed on $LiNi_{0.5}Mn_{1.5}O_4$ (LNMO) and graphite is being analysed along with intermittent current interruption (ICI) technique to observe the resistance while cycling. The results show that the sulfolane electrolyte shows more degradation at higher potentials unlike previous reports which suggested higher oxidative stability. However, the passivation layers formed due to this electrolyte degradation prevents further degradation. The resistance measurements show that major resistance arises from the cathode. The pressure evolution during the formation cycles suggests that there is lower gas evolution with sulfolane electrolyte than in the conventional electrolyte. The study opens a new outlook on the sulfolane based electrolyte especially on its oxidative/anodic stability.

Introduction

The demand for high-power and high-energy density battery applications such as electric vehicles has enhanced the growing interest in exploring different cathode materials for lithium-ion batteries. In particular, high-voltage cathode materials like lithium nickel oxide ($LiNiO_2$), lithium cobalt phosphate ($LiCoPO_4$) and lithium nickel manganese oxide ($LiNi_{0.5}Mn_{1.5}O_4$; LNMO) have been explored as potential cathodes for high-energy density applications.[1,2] LNMO has attracted a special interest in last few years due to its high-voltage (4.7 V vs. Li/Li^+), promising theoretical capacity of 147 mAh/g, and its stable spinel structure that allows excellent rate capabilities.[3–7] The absence of cobalt, which is an expensive and less abundant metal facing increasing demands,[1] makes LNMO prominent among the inorganic high-voltage cathode materials. However, the lower anodic stability of the conventional electrolyte solutions based on ethylene carbonate (EC) (>4.3 V vs. Li/Li^+)[8,9] restricts the full potential of LNMO. The polycarbonate layer formed during the formation cycles becomes unstable at higher potentials, paving the way for gas evolution and other undesired side-reactions, thereby leading to capacity fade.[9,10] Hence, the use of EC-free electrolytes has appeared as a strategy to formulate electrolytes for high-voltage cathodes.[11]

In this context, studies have been reported on potential electrolytes that are more stable at higher voltages. Electrolytes with sulfones,[12] nitriles,[13] ionic liquids,[14] fluorinated carbonates[15] have been explored with/without co-solvents to decrease their viscosities. Sulfolane has been used both as an additive[16] in conventional electrolytes to raise the oxidation potential of the electrolyte, but also as a sole aprotic solvent in the electrolyte[17,18] or used with a co-solvent.[19–24] Sulfolane exhibits a high boiling point of 287 °C, a flash point of 165 °C and a dielectric constant of >40, primarily due to the oxygen in the sulfone group which is the coordinating motif to the lithium ion, and which triggers dissolution of lithium salts.[8,11,18]

With respect to the conducting salt, lithium bis(fluorosulfonyl)imide (LiFSI) has a thermal stability of 200 °C and high solubility in organic solvents.[25] Since fluorine in LiFSI has a lower tendency to form hydrogen fluoride compared to that in the conventional electrolytes containing lithium hexafluorophosphate ($LiPF_6$), the transition metal dissolution occurring in LNMO at higher potentials can be decreased.[8] It has been shown that in the presence of LiFSI salt, an effective solid-

[a] Dr. G. D. Salian, A. Mathew, Dr. R. Gond, W. van Ekeren, Prof. D. Brandell, Assoc. Prof. R. Younesi
Department of Chemistry-Ångström Laboratory
Uppsala University
Box 538, SE-75121 Uppsala (Sweden)
E-mail: reza.younesi@kemi.uu.se
[b] Dr. J. Højberg, Dr. C. Fink Elkjær
Haldor Topsøe A/S
Haldor Topsøes Allé 1, DK-2800 Kgs, Lyngby (Denmark)
[c] Dr. M. J. Lacey
Scania CV AB
SE-15187 Södertälje (Sweden)
[d] Dr. S. K. Heiskanen
Volkswagen AG
D-38436 Wolfsburg (Germany)

Supporting information for this article is available on the WWW under https://doi.org/10.1002/batt.202200565

An invited contribution to a Special Collection dedicated to NordBatt 2022 conference

electrolyte interface (SEI) layer is formed on graphite which prevents this exfoliation, rendering the combination of SL and LiFSI particularly appealing.[19,26] Concentrated electrolytes containing LiFSI salt also showed passivation layers being formed on the aluminium (Al) current collector that prevented its corrosion.[17,27] As high salt concentration accompanies with higher cost, we here investigate the use of sulfolane based electrolyte containing LiFSI salt with the commonly used "standard" concentration of 1 M for electrochemical cycling of LNMO-graphite cells.

Studies on the anodic stability of sulfolane based electrolytes have commonly used techniques like cyclic voltammetry (CV) and linear sweep voltammetry (LSV).[11,17] These techniques are governed by their sweep/scan rates that do not match the actual cycling of a cell (half or full cell) spending lower time at the redox plateaus. Hence a clear understanding on the anodic/oxidative stability is not achieved while using these electrochemical techniques. This study incorporates the use of an electrochemical method called synthetic charge-discharge profile voltammetry (SCPV)[28] to understand the anodic stability of the sulfolane based electrolyte in comparison to the conventional electrolyte. This in combination with passivation layer study using X-ray photoelectron spectroscopy (XPS) reveal important perspectives with regards to this electrolyte in a full cell chemistry of LNMO-graphite. The resistance increment with cycle number is measured using the intermittent current interruption (ICI) technique, which shows the dynamic resistance change while galvanostatic cycling.[29] The formation cycles involving the gas evolution is a crucial step that occurs in the first few cycles. The pressure evolution of the full cells with sulfolane electrolyte and conventional electrolyte during the formation cycles is also assessed.

Results and Discussion

Sulfolane is a solid at room temperature and hence it was melted at 40 °C and mixed with the LiFSI salt. The viscosity of such a solution is high which can affect the ionic conductivity. Figure 1(a) shows the ionic conductivity of 1 M LiFSI in SL electrolyte in the temperatures range of 25 °C to 55 °C. The ionic conductivity at 25 °C is around 3 mS cm^{-1}, which is lower than that of conventional carbonate based liquid electrolytes, i.e., 10 mS cm^{-1}.[11] The lower ionic conductivity of sulfolane is correlated to its high viscosity when it is not combined with any co-solvent.

The electrochemical stability window of the sulfolane electrolyte was investigated using different methods, and the shortfall conventional CV is here discussed. Figure 1(b) shows CV of a half-cell with C-coated Al foil as the working electrode where the potential was linearly swept up to 5.5 V (see Figure 1b). The increase in current starts around 4.5 V in the first oxidation cycle, which is likely originating from a combination of electrolyte decomposition, oxidation of functional groups on the carbon coating and oxidation of possible impurities. While the oxidation is expected to decrease in the following cycles, Figure 1(b) instead displays that the oxidation current actually increases from the 1st to 5th cycle. This increase suggests that the decomposition products do not form any efficient passivation layer to suppress parasitic oxidation reactions. Similarly, a half-cell of LNMO *vs.* Li-metal also showed an increase in the current during from the 1st to 5th cycle (see Figure S1a). At the same time, the CV of LNMO-graphite full cells did not show any such increase in oxidation current by the number of cycle (see Figure S1b). This suggests that the counter electrode plays a role in the oxidation current measured on the working electrode, which indicates that there exists a 'cross talk' between the electrodes, i.e., the decomposition products formed on Li-metal counter electrode in the half-cells diffuse to the surface of working electrode where their oxidation leads to an increased current. Hence a half-cell with lithium counter electrode does not accurately determine the stability of the electrolyte.

In CV or linear sweep voltammetry (LSV) experiments, the time spent by the cell at a particular potential is governed by the sweep rate and is not in accordance with a 'real' cell when cycled in a galvanostatic cycling test, where the time spent by the electrolyte at the plateau or at a higher potential is more

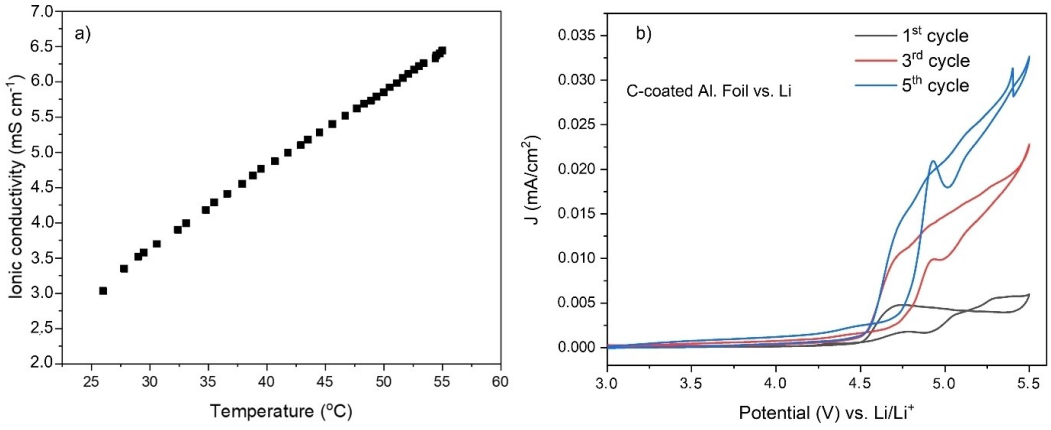

Figure 1. a) The ionic conductivity of 1 M LiFSI in sulfolane electrolyte in the range of 25 °C to 55 °C; b) CV of C-coated Al foil vs. Li recorded at a scan rate of 0.05 mV/s between 3.0 V and 5.5 V.

Research Article
doi.org/10.1002/batt.202200565
Chemistry Europe
European Chemical Societies Publishing

than in a CV or LSV. Hence to obtain a better understanding of the anodic stability of 1 M LiFSI in sulfolane electrolyte, SCPV experiments were performed with C-coated Al as the working electrode in a 3-electrode cell with delithiated LFP as counter and reference electrodes as mentioned in the experimental section. The SCPV technique controls the voltage in such a way that it follows the voltage profile of an active material of interest (LNMO in this case), and thereby provides realistic operational conditions in terms of the voltage changes with time which mimics that of a real LNMO battery. As shown in Figure 2(a), during the initial SCPV anodic scan, the cell with sulfolane electrolyte passed a total of ~7 μAh cm^{-2} charge, whereas the cell with LP40 electrolyte delivered ~5 μAh cm^{-2}. The quantity of charge passed is an indication of the amount of electrolyte degradation in the cell. Note that in the lower plateau region, i.e., lower than 0.9 V, corresponding to the 4.0–4.1 V plateau which is equivalent to the Mn^{3+}/Mn^{4+} redox couple in an LNMO half-cell (0.6–0.7 V in this case where the potential is versus LFP), a smaller quantity of charge is passed in the sulfolane electrolyte than in LP40. In a previous publication,[28] a higher quantity of charge was detected in the lower plateau region in a 1 M $LiPF_6$ + SL electrolyte than in LP40, which was then attributed to sulfolane decomposition. The increased quantity of charge there could have originated from either $LiPF_6$ salt or an unknown impurity, since the corresponding system with LiFSI salt does not display any similar behavior.

The differential plot (d*Q*/d*E* vs. *E*) in Figure 2(b) aids a better visual representation of the *Q* vs. E plot. The two peaks in the 1.2–1.4 V range demonstrate that the electrolytes degrade more rapidly in the upper plateau region, i.e. above 0.9 V, which corresponds to more time spent at higher voltages associated to Ni^{2+}/Ni^{3+} and Ni^{3+}/Ni^{4+} redox couples. A higher degradation is then observed for the sulfolane based electrolyte than when using LP40.

For both cells, SCPV scans were run for multiple cycles as shown in Figure 3(a). The amount of charge passed in the lower (< 0.9 V) and upper (> 0.9 V) plateau regions for sulfolane and LP40 electrolytes, respectively, for up to 12 cycles are presented in Figure 3(b and c). The amount of charge passed in the lower plateau region is shown in Figure S2 for both the electrolytes. Apart from the initial cycles, the amount of charge in subsequent cycles does not rise significantly, indicating that a stable passivation layer is formed. For each cycle, the sulfolane-based cell display a higher quantity of charge compared to the LP40-based cell, which could explain the lower coulombic efficiency (CE) observed in the sulfolane-based cell, which is further discussed in the context of Figure 4.

LNMO-graphite full-cells were cycled with the sulfolane and the LP40 electrolytes using a formation cycle for 3 cycles at C/10 rate and then successive cycles up to 100 cycles at C/3 for constant current-constant voltage (CC–CV) conditions. Before the cell cycling, for both the cells with the respective electrolytes, a constant voltage step at 1.2 V was applied. This step is usually performed in Li-ion cells primarily to ensure complete wetting and avoid Cu dissolution during the rest period before cycling.[30–33] The effect of such a step is shown in Figure 4(a and b), wherein the LNMO-graphite full-cells containing sulfolane electrolyte are compared with and without the constant voltage step at 1.2 V. The cell held at 1.2 V before cycling shows higher discharge capacities (Figure 4a) than the one held at open circuit voltage (OCV). Both cells show a similar trend in the capacity fade. The initial capacities of both the cells increases with cycles, probably due to poor initial wetting of the electrodes due to the viscosity of the electrolyte. The CE of the cell employing the constant voltage step are slightly higher, reaching up to 99.5% at the end of 100 cycles. Figure 4(c) shows a comparison of discharge capacities of LNMO-graphite cells containing sulfolane and LP40 electrolytes. Here, the cells containing sulfolane and held at 1.2 V is compared with the cell with LP40, also held at 1.2 V constant voltage before cycling. The discharge capacities are obviously higher for the cell with sulfolane than that with the LP40. Also, the trend in the capacity fade is higher for LP40 electrolyte.

The results show the positive effect of the constant voltage step at 1.2 V for the cell with sulfolane electrolyte, but the CE is slightly lower to the cell with LP40. The degradation of the sulfolane electrolyte at higher potentials as observed in the

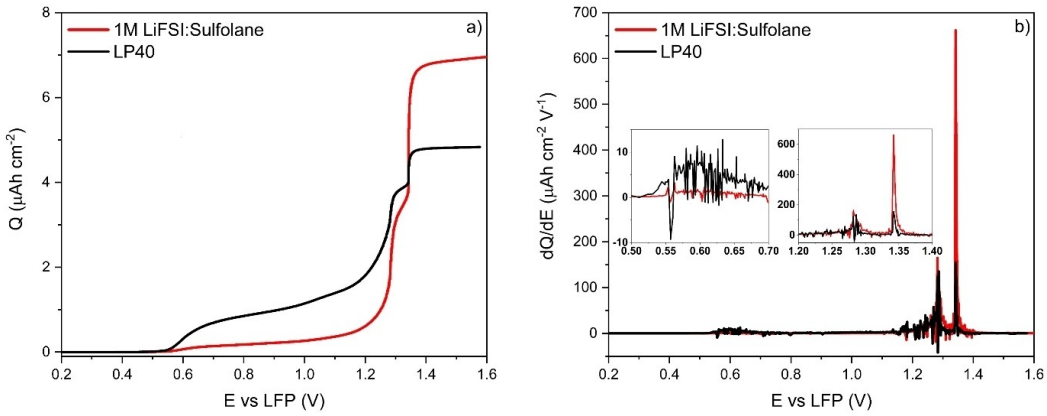

Figure 2. a) The amount of charge passed for sulfolane and LP40 based cells in the first anodic sweep of the SCPV method (*Q* vs. *E*) and b) the corresponding differential plot (d*Q*/d*E* vs. *E*).

Research Article
doi.org/10.1002/batt.202200565
Chemistry Europe
European Chemical Societies Publishing

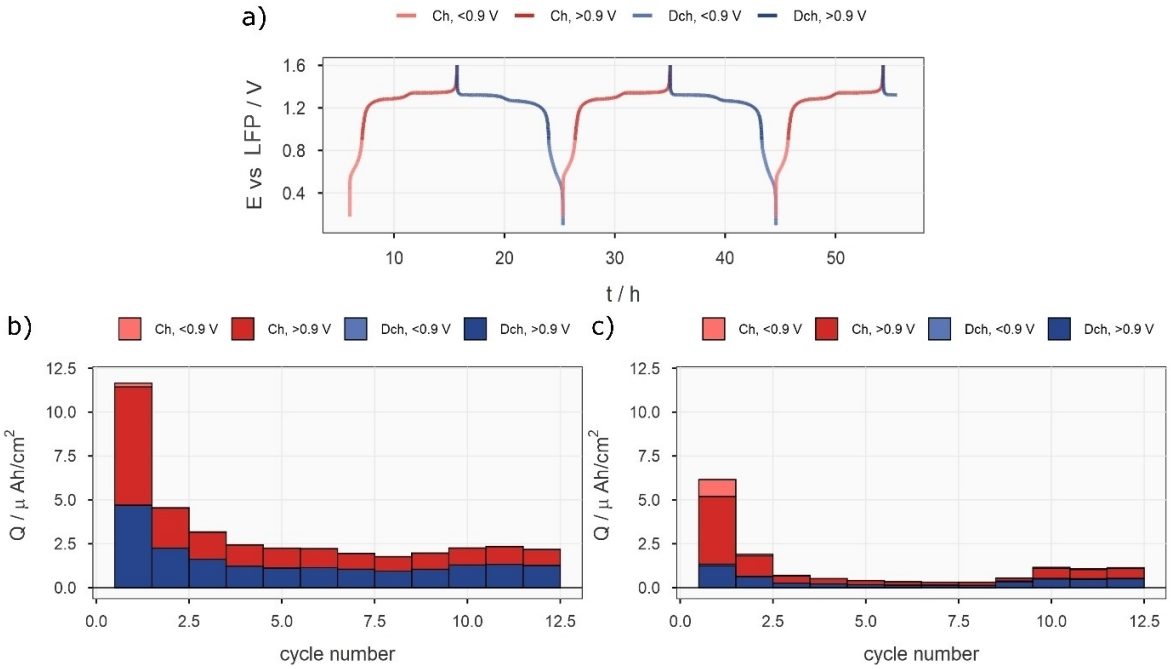

Figure 3. a) Voltage profile of an LNMO half-cell with different voltage regions marked. Multiple SCPV cycles for b) sulfolane:LiFSI and c) LP40.

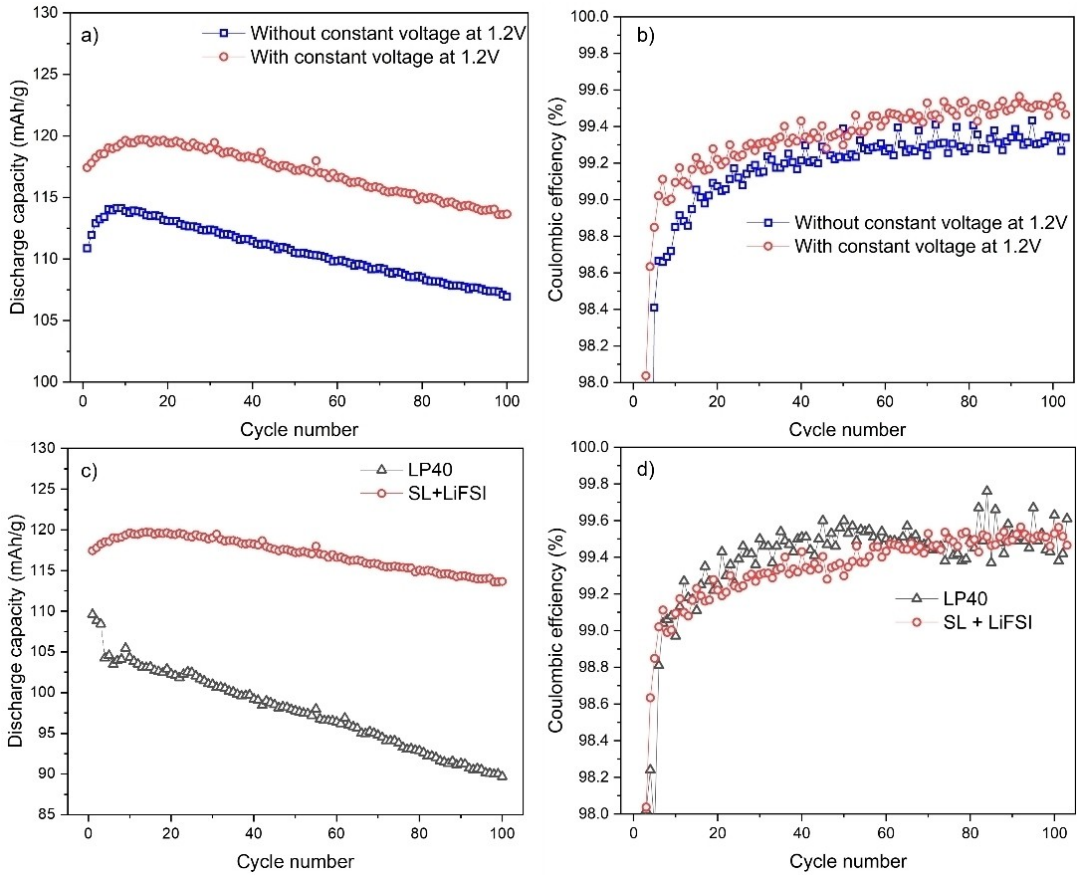

Figure 4. a) Discharge capacities and b) CE of LNMO-Graphite cells in sulfolane electrolyte with and without constant voltage at 1.2 V; c) Discharge capacities and d) CE of LNMO-Graphite cells in sulfolane electrolyte and LP40 with constant voltage at 1.2 V.

Research Article
doi.org/10.1002/batt.202200565
Chemistry Europe
European Chemical Societies Publishing

SCPV measurements could be the reason for a slightly lower CE. That said, the discharge capacities are higher for the cell with sulfolane electrolyte than the one with LP40. Hence the passivation layer formed due to the degradation of the sulfolane electrolyte could have aided in lower degradation of the electrolyte and the efficient Li-ion conduction. More so, the constant voltage step at 1.2 V before cycling could have enabled another thin layer that would have aided in lower degradation of the sulfolane electrolyte and hence improved CE.

Figure 5(a and b) shows the charge-discharge cycles for LNMO-graphite full cells with sulfolane and LP40 electrolytes, respectively. The first three formation cycles at C/10 and 4th, 53rd and 103rd cycles for both cells are shown. The overpotential is higher for the cycles both at C/10 and C/3 for the cell with sulfolane electrolyte as compared to that with LP40. The ionic conductivity is likely a major factor contributing to the higher overpotential for the cell with sulfolane electrolyte. However, the discharge capacities were higher and more stable up to 100 cycles for the same cell. This could possibly indicate lower loss of cyclable lithium for the case of sulfolane electrolyte in contrast to the cell with LP40 electrolyte. This is even more evident when both cells are cycled up to 500 cycles (Figure 5c); i.e., the capacity retention for the cell with sulfolane is significantly better than that for LP40. While the cell with sulfolane does show some capacity fade, the major capacity fade starts after 200 cycles, whereas the capacity fade of the LP40 cell starts from the very beginning.

Galvanostatic cycling tests were accompanied with the resistance measurements. This was done in a three-electrode cell, as explained in the experimental section, to determine which component of the cell contributed to the resistance (see Figure 6). The first cycle shows a higher resistance for both electrolytes, which is primarily originating from the LNMO electrode (Figure 6a and e). This could indicate CEI layer formation or oxidation reactions relating to the binder. This is corroborated in the SCPV measurements with the electrolyte degradation in the first cycle for both sulfolane and LP40, more so for sulfolane electrolyte (Figure 2a). The resistance then decreases in subsequent cycles for both cells, still with the resistance contributions from the graphite electrode being comparatively small. On the graphite anode, where reduction takes place in the first cycle, the first discharge displays a higher resistance during this process, which can be seen in Figure 6(b and f) for cells in sulfolane and LP40, respectively. This indicates SEI layer formation in both types of cells caused by electrolyte reduction.

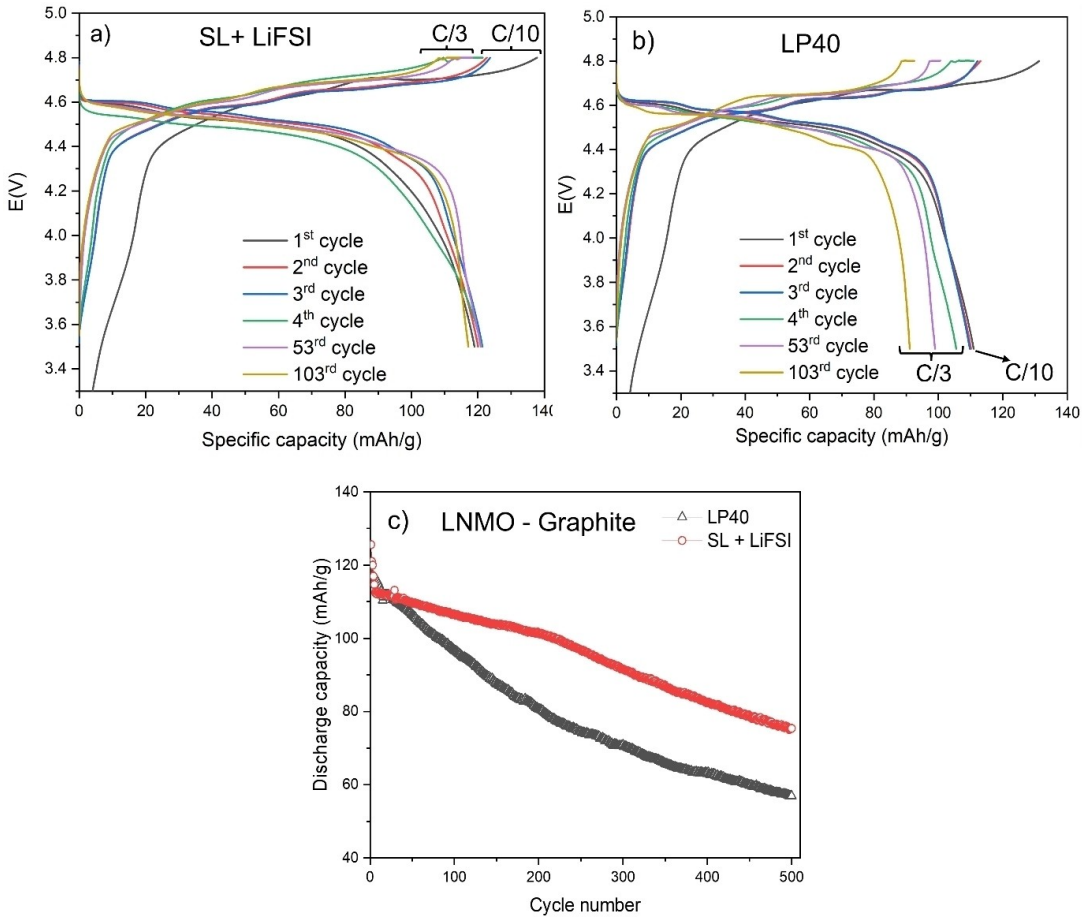

Figure 5. Charge-discharge curves at C/10 (formation) and C/3 rates for LNMO-Graphite full cells in a) sulfolane electrolyte, b) LP40 electrolyte, c) long-term cycling tests up to 500 cycles.

Research Article
doi.org/10.1002/batt.202200565
Chemistry Europe
European Chemical Societies Publishing

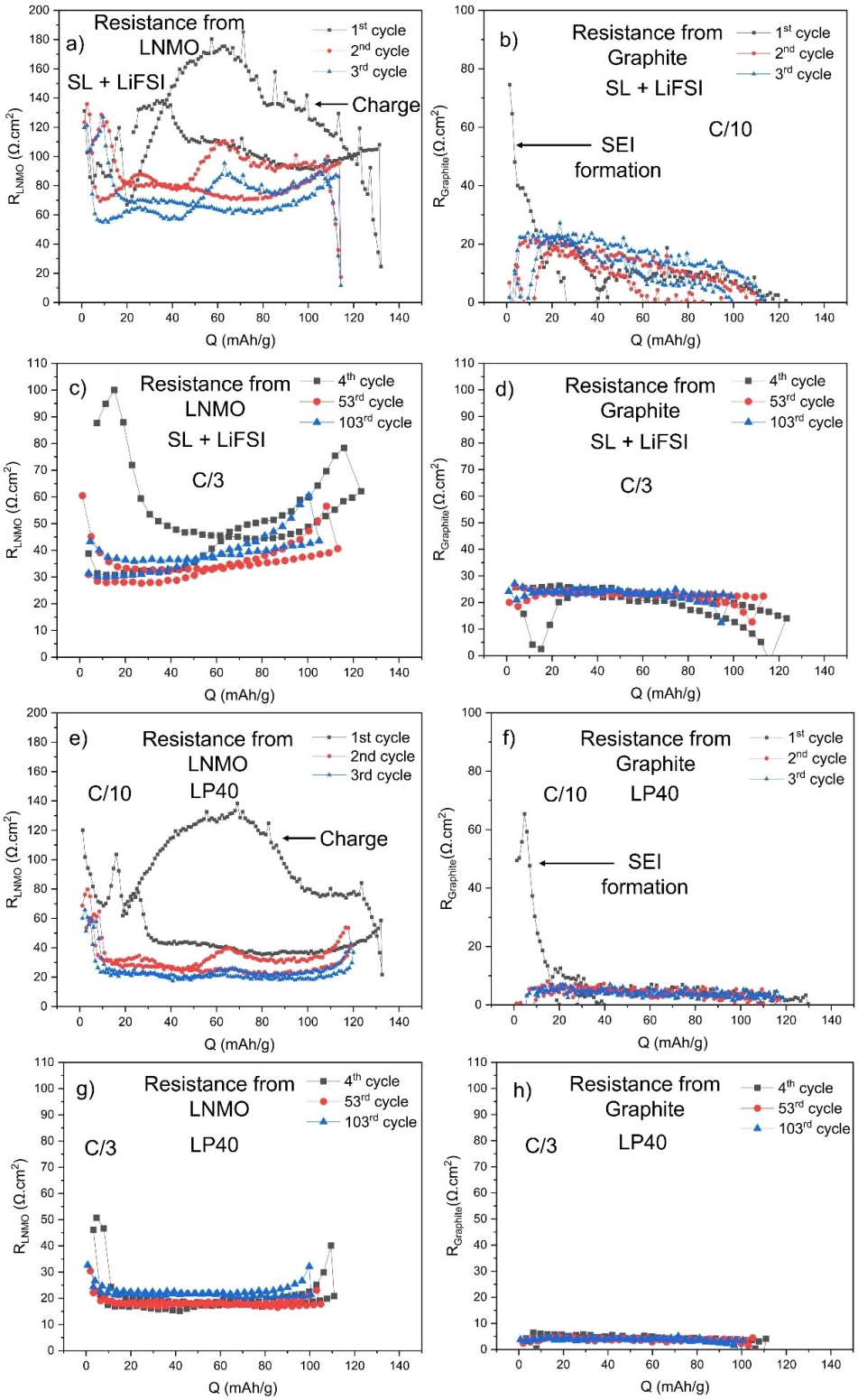

Figure 6. ICI analysis in 3-electrode cells of LNMO-graphite with delithiated LFP as reference. a) Resistance from LNMO and b) resistance from graphite during the formation cycles at C/10 rate; c) resistance from LNMO and d) resistance from graphite during the during the subsequent cycling at C/3 rate up to 100 cycles in sulfolane electrolyte; e) resistance from LNMO and resistance from graphite during formation cycles at C/10 rate in LP40 electrolyte; g) resistance from LNMO and h) resistance from graphite during subsequent cycling at C/3 rate up to 100 cycles in LP40 electrolyte.

After these formation cycles, the cells were cycled at C/3 rate up to 100 cycles. The resistance increases in both cells, with the major resistances originating from the LNMO electrode (Figure 6c and g). The graphite electrode contributes with very

Research Article
doi.org/10.1002/batt.202200565
Chemistry Europe
European Chemical Societies Publishing

low resistances for both electrolytes, as seen in Figure 6(d and h). After several cycles, the cell with sulfolane electrolyte, however, shows overall higher resistance than the cell with LP40, most likely due to the lower ionic conductivity of sulfolane than for LP40.

As indicated in the ICI measurements, the passivation layers (CEI and SEI) are formed on both the cathode and the anode. To determine the nature of these passivation layers, XPS analysis was performed on LNMO and graphite electrodes after 100 cycles and they were compared to their respective pristine electrodes. The survey spectra shown in Figure S4 display that the Na 1s peak, which originates from the binder and is clearly detectable in the pristine samples, is diminished in the cycled electrodes. This indicates that a surface layer thicker than 10 nm is formed on both electrodes, as the excitation energy used was 1486.6 eV Al K_α radiation which has probing depth of ~11 nm.[34] The C 1s, O 1s, F 1s, and S 2p spectra presented in Figure 7 reveal formation of variety of decomposition products on the surface of the electrodes (also tabulated in Table S1). C 1s of both LNMO and graphite electrodes from the cell with LP40 electrolyte depict similar species.[35] In summary, the C 1s spectra of LNMO electrodes indicate that the surface layer is more hydrocarbon-rich when sulfolane is used, and more ether-species when LP40 is used. As shown in Figure 7(a and e), the C 1s spectra for LNMO and graphite display a more pronounced peak at 284.8 eV in sulfolane for hydrocarbon rich species and 287 eV in LP40 cycled electrodes witnessing SEI/CEI is ether rich species, respectively.[36]

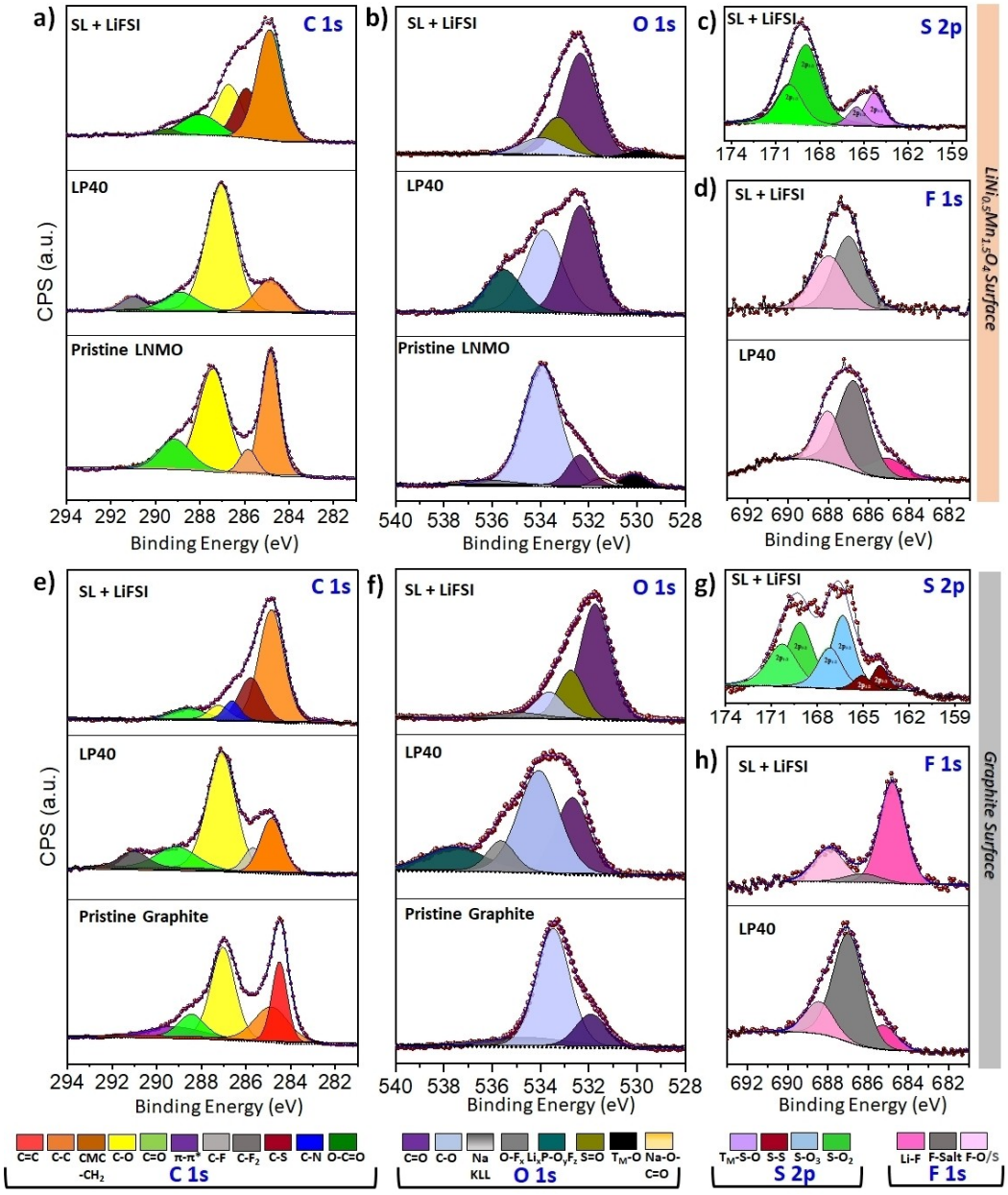

Figure 7. XPS spectra of pristine and cycled LNMO and graphite electrodes cycled in sulfolane and LP40 electrolytes.

Research Article
doi.org/10.1002/batt.202200565
Chemistry Europe
European Chemical Societies Publishing

O 1 s spectra in the cycled LNMO electrodes showed suppression of T_M–O bond signals as compared to the pristine LNMO electrode advocating the presence of a surface layer in the cycled electrodes, which is of thicker nature in LP40 than sulfolane supporting the presence of thick CEI in LP40 causing very diminished peak at 529.6 eV for T_M–O bond (Figure 7b).[17] Similar decomposition products were seen in sulfolane electrolyte on both LNMO and graphite cycled electrodes. The ratio between C–O and C=O in LNMO and graphite exhibits similar feature (Figure 7b, f topmost images) witnessing hydrocarbon rich CEI/SEI derived from FSI^- and tetramethylene sulfone and being carbonate impoverished. On the graphite surface the O 1 s spectra in Figure 7(f) in the pristine electrode, the inherent C–O and C=O peaks at 533.4 eV and 531.9 eV, respectively, are found to be shifted to 534 eV for C–O and 532.6 eV for C=O in LP40 (more polymeric in nature), while for sulfolane the C–O and C=O was seen at 533.6 eV and 531.6 eV along with the S=O peak at 532.8 eV. Sulfolane cycled LNMO and graphite S 2p comprised of majorly pristine imide salt as well as few FSI^-/sulfolane decomposition products shown in Figure 7(c and g), respectively. On the LNMO surface the S species are predominantly pristine imide salt ($S\,2p_{3/2}$ 168.9 eV) along with some T_M–S–O ($S\,2p_{3/2}$ 164.25 eV), however the graphite surface showed the presence of pristine imide salt ($S\,2p_{3/2}$ 169.1 eV) as well as some decomposed Li-imide salt ($S\,2p_{3/2}$ 166.3 eV) along with the S–S species ($S\,2p_{3/2}$ 163.9).[37,38] On the other hand the salt decomposition can also be easily seen in F 1 s spectra in Figure 7(d and h) which showed huge dissimilarity for sulfolane and LP40-based cycled electrodes, respectively. LNMO and graphite surface cycled in LP40 are almost identical with predominant feature of Li_xPF_y and $Li_xPF_yO_z$ and very little LiF.[37–39] However, the sulfolane cycled LNMO and graphite electrodes showed huge difference, where CEI is mainly composed of FSI^- based species and SEI is LiF rich, thus more stable SEI causing more Li-ion transport in sulfolane.[40] Thus, F 1 s spectra discloses that a relatively higher amount of LiF is present on the surface of the graphite electrode cycled in sulfolane. Based on previous research and the current findings, it is clear that the interface in LP40 is polymeric (ether rich) and deprived of LiF, whereas the SEI in LiFSI + sulfolane-based electrolytes is more inorganic (hydrocarbon rich with LiF enrichment), which is not dynamic like carbonate-based electrolytes. Hence higher cycle stability in seen in a LNMO-graphite cell with sulfolane based electrolyte.[41,42]

SEM analysis was performed on pristine and cycled LNMO and graphite electrodes to observe any morphology changes after cycling. Figure S5 shows the SEM images of pristine and cycled LNMO and graphite electrodes after 100 cycles both in sulfolane and LP40 electrolytes. The pristine LNMO electrode (Figure S5a) shows the LNMO particles of approximately 5 μm size surrounded by the network of carbon additives and binder. It is interesting that there are no morphology changes observed for the LNMO electrodes after cycling either in sulfolane or LP40 electrolytes. The pristine graphite electrode, in turn, shows a particle size between 10–12 μm. Like LMNO, the cycled graphite electrodes show no morphology change at this length scale upon cycling.

A pressure evolution study was also performed for the LNMO-graphite cells cycled in both sulfolane and LP40 electrolytes, whereby the pressure evolution was monitored during the first three formation cycles. Especially during the formation cycles (here at C/10), the electrolyte is being reduced on the anode and oxidized on the cathode (as shown in SCPV measurements as increase in amount of charge and in the ICI measurements as increase in resistance). Although these electrolyte/electrode reactions are to some extent beneficial, they can also lead to the formation of undesired gaseous, solid, and liquid products which can cause cell failure.[43]

In Figure 8(a and b), the time-dependent full-cell potential and corresponding pressure curve is shown for the formation cycles. The pressure evolution over time, here expressed as $\triangle P$ (mbar), is obtained by subtracting the stabilized absolute pressure (after being kept 10 hours at OCV conditions) with the absolute pressure increase. The cell using the LP40 electrolyte has a significant pressure increase in the first cycle, approximately 16 mbar. The gas evolution continues during the subsequent cycles, although the evolution rate decreases to about 1–2 mbar per subsequent cycle. For the cell using the sulfolane based electrolyte, the gas evolution is comparatively small. The pressure increase is approximately 6 mbar and mainly takes place during the first charge, after which the pressure stabilizes. It could be deduced that the reactions during the formation cycles with sulfolane evolve lower volume of gases, though the SCPV results suggest higher degradation

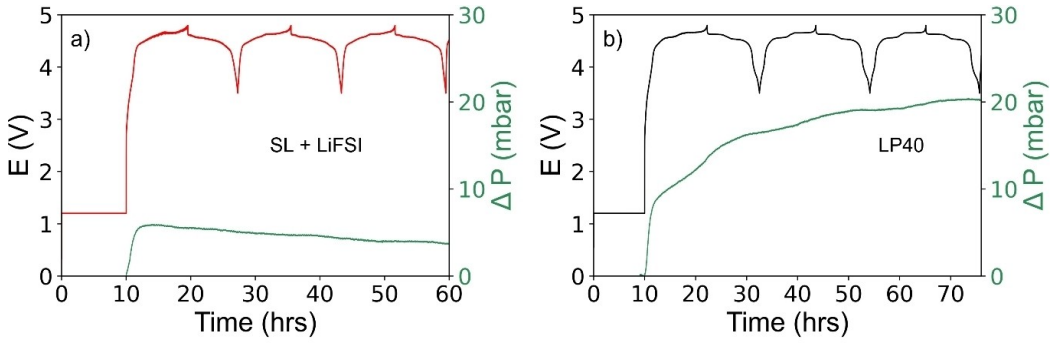

Figure 8. Formation cycles and pressure evolution for a LNMO-graphite cell with a) 1.0 M LiFSI in sulfolane and b) LP40 electrolyte.

of sulfolane. This therefore suggests that the degradation reactions contribute in formation of solid or liquid rather than gaseous species, and such species may contribute in building robust CEI/SEI layers. The pressure evolution analysis was also accompanied by ICI resistance measurements in the pressure cell (PAT) (Figure S3). The resistance values from this measurement shown in Figure S3 disclose a similar trend as in Figure 6; i.e., the cell sulfolane electrolyte showed higher resistance values compared to the cell with LP40 electrolyte. So, the pressure evolution does not appear to have had any significant impact on the resistance measurements. Overall, it can be concluded that the pressure evolution in LNMO-graphite cells with sulfolane based electrolytes can be significantly reduced compared to using conventional LP40 electrolyte.

Conclusion

The electrolyte solution of 1 M LiFSI in sulfolane provides ionic conductivity of 3 $mS\,cm^{-1}$ at 25 °C which is lower than that of LP40 electrolyte. The sulfolane electrolyte, compared to LP40, also suffers from higher degree of degradation at higher potentials. However, a constant voltage step of 1.2 V applied before cycling shows an improvement in the discharge capacities and CE for the cell with sulfolane. This is attributed to the formation of a thin layer suppressing further degradation of sulfolane at higher potentials. Therefore, the charge-discharge cycles for the cell with sulfolane show higher stability than that of LP40. XPS analysis on LNMO and graphite cycled for 100 times revealed that the CEI layer is hydrocarbon-rich in sulfolane based cell while it is more ether-rich for in the cell with LP40 electrolyte. The composition of SEI on graphite was inorganic (LiF) rich in the cell with sulfolane electrolyte while it was more ether rich in the cell with LP40. The ICI resistance measurements indicated that the resistance arises from the LNMO electrode in both the electrolytes, however the cell with sulfolane electrolyte showed higher resistance, originating from the lower ionic conductivity and higher viscosity of the electrolyte. Pressure evolution studies in PAT-cells of the full-cells revealed that the gas pressure increases more for LP40 during the formation cycles than for that of sulfolane electrolyte. The work suggests that even though being a viscous electrolyte, SL + LiFSI electrolyte can provide higher cycle stability in a LNMO-graphite cell, which is likely due to better passivation layers obtained on the electrodes.

Experimental

LNMO powder was obtained from Haldor Topsøe A/S, Denmark. The LNMO composite electrodes were fabricated by mixing a slurry containing the active material powder with Super P conductive carbon and CMC binder at a weight ratio of 90:5:5 using a MM mixer mill (Retsch) at 25 Hz for 30 min with de-ionized water as the solvent for blending the electrode mixture. The obtained slurries were then casted onto carbon-coated Al foil (20 μm thick) using a doctor blade. The coatings were then dried at 75 °C overnight. Electrodes of diameter 20 mm were punched from the coatings and were calendared at a pressure of 1.59 $ton\,cm^{-2}$. The calendared LNMO composite electrodes were then dried in a Büchi oven at 120 °C for at least 12 h. The active mass loading was around ~10.5 $mg.cm^{-2}$ (or 1.5 $mAh\,cm^{-2}$). Graphite powder was obtained from Imerys (GDHR 15-4 graphite). The graphite electrodes were obtained by coating the aqueous slurry of graphite powder, C65 carbon black and CMC binder in the ratio of 92:3:5 respectively, on a C-coated Cu foil. The coatings were then dried at 75 °C overnight. Graphite electrodes of 20 mm were punched out and then dried in a Büchi oven in an Ar-filled glovebox at 120 °C for at least 12 h. The coated graphite electrode had a mass loading of 5.3 $mg\,cm^{-2}$ (or 1.8 $mAh\,cm^{-2}$).

To prepare the electrolyte, tetramethylene sulfone or sulfolane obtained from Sigma Aldrich was melted to 40 °C in argon filled glovebox, and then dried while molecular beads were added into the bottle and kept for one week to absorb any water content from the solvent. After this, a calculated amount of the solvent was taken and 1 M LiFSI (Provisco) was added into the sulfolane solvent and stirred in the glovebox for 24 hours. To check the ionic conductivity of the obtained electrolyte, measurements were performed using a Mettler Toledo SevenGo Duo pro pH/ORP/Ion/Conductivity meter SG78 with an InLab 738ISM probe under argon in a glovebox from room temperature to 55 °C.

For SCPV measurements[28] a three-electrode cell was assembled with C-coated Al foil as the working electrode and delithiated (until 3.4 V) lithium iron phosphate (LFP) as both the counter and reference electrode in a pouch cell using glass fiber and Celgard separators respectively for sulfolane and LP40 based cells. 150 μL of electrolyte were used in each cell.

Delithiated LFP was obtained from a half-cell cycled with LP40 as the electrolyte. The half-cell was cycled between 3.0 V and 4.2 V in the first cycle and then charged up to 3.4 V. After that, the cell was disassembled in the glovebox and washed with dimethyl carbonate (DMC) and dried to obtain the delithiated LFP. LFP was chosen as a reference electrode due to its stable nature against the electrolyte. The LNMO voltage profile was obtained by cycling an LNMO | LP40 | Li cell at room temperature in the voltage range of 3.5 to 5.0 V on an Arbin BT cycler, USA at C/10 rate. The resultant voltage profile was then modified by subtracting 3.4 V (LFP voltage plateau) to correspond to a full-cell in the 0.1–1.6 V range. The SCPV measurements were performed according to a procedure described in a previous publication.[28] The CV measurements were performed on a VMP2 Biologic potentiostat, in the potential range of 3.0–5.5 V at a scan rate of 0.05 mV/s. The ICI measurements for internal resistance measurements were tested in a three-electrode system in a pouch cell wherein the working electrode was LNMO, the counter electrode was graphite, and the reference electrode was delithiated (until 3.4 V) LFP with sulfolane and LP40. The employed ICI method was consisting of 1 s rest at 2 min intervals is described in further detail in.[29]

The electrochemical performance of the LNMO-graphite full cells was tested in pouch cells with sulfolane electrolyte and LP40 electrolyte respectively in a voltage range of 3.5–4.8 V on a BT-2000 Arbin tester, USA. The pouch cells for CV, ICI, SCPV and for testing the electrochemical performance, were assembled in an argon filled glovebox (MBraun) with H_2O and O_2 < 1 ppm. These tests were done at room temperature.

Electrode morphologies were imaged via a Zeiss 1550 scanning electron microscope (SEM). For post-mortem analysis, pouch cells cycled in sulfolane and LP40 electrolytes were opened in an Ar-filled glovebox. LNMO and graphite electrodes were then rinsed with DMC five times using 4–5 droplets each time to remove salt residues. Electrodes were placed on carbon tapes after drying off

the DMC. Samples were transferred to the SEM in airtight glass vials and exposed to air for 15–20 s before being transferred to the SEM chamber. The accelerating voltage was 10 kV.

Surface characterization was performed through X-ray photoelectron spectroscopy (XPS). The procedure for sample preparation was the same as for SEM and an airtight transfer system was used for the samples to avoid any exposure to air. Pristine and cycled LNMO and graphite electrodes were analyzed using a Phi-5500 instrument with monochromatized Al $K\alpha$ radiation (1486.6 eV). Data calibration was made by linear shifting of the hydrocarbon peak to 284.8 eV. CasaXPS was used for the analysis of the XPS data.

Pressure monitoring of the cells was performed in a helium-leak tested pressure cell (PAT-Cell-Press) of El-Cell® GmbH. The PAT-Cell-Press consists of a lower plunger, upper plunger and insulation sleeve which were all used as delivered by El-Cell. The plungers are respectively made of aluminium and copper, acting as current collectors. The insulation sleeve contains the pre-dried 260 μm borosilicate-glass fiber separator which has a diameter of 18 mm (GF/A of Whatman®, UK). LNMO and graphite electrodes were punched to a diameter of 18 mm and dried under vacuum at 120 °C. The cell setup was helium leak tested and guaranteed a minimum leakage rate of 0.3 mbar/hour. The separate cells containing sulfolane and LP40 electrolyte were assembled with 100 μL electrolyte in an argon-filled glovebox (MBraun). After assembly, the cells were placed in a climate chamber (KB53, Binder® GmbH) and cycled at 30 °C using a Biologic potentiostat. The cells were cycled up to 3 cycles (formation cycle at C/10) employing the ICI technique with 1 s rest in 2 min interval. The lower and upper cut-off potentials were respectively 3.5 V and 4.8 V.

Acknowledgements

The authors acknowledge the financial support from Haldor Topsoe A/S, Denmark, from the Swedish Energy Agency via project no. 45518-1, via STandUP for Energy, and from CoFBAT, which is an EU-funded project that has received funding from the European Union's Horizon 2020 Research and Innovation Programme under Grant Agreement N. 875126.

Conflict of Interest

Some of the co-authors are from industrial partners including Volkswagen, Scania and Haldor Topsøe

Data Availability Statement

The data that support the findings of this study are available from the corresponding author upon reasonable request.

Keywords: anodic stability · ethylene carbonate-free electrolyte · graphite · lithium-ion battery · $LiNi_{0.5}Mn_{1.5}O_4$ · passivation layers · sulfolane

[1] W. Li, B. Song, A. Manthiram, *Chem. Soc. Rev.* **2017**, *46*, 3006.
[2] W. Lee, S. Muhammad, C. Sergey, H. Lee, J. Yoon, Y. Kang, W. Yoon, *Angew. Chem.* **2020**, *132*, 2598–2626; *Angew. Chem. Int. Ed.* **2020**, *59*, 2578–2605.
[3] C. M. Julien, A. Mauger, *Ionics* **2013**, *19*, 951–988.
[4] B. Aktekin, M. J. Lacey, T. Nordh, R. Younesi, C. Tengstedt, W. Zipprich, D. Brandell, K. Edström, *J. Phys. Chem. C* **2018**, *122*, 11234–11248.
[5] M. Zhang, N. Garcia-Araez, A. L. Hector, *J. Mater. Chem. A* **2018**, *6*, 14483–14517.
[6] N. Tolganbek, Y. Yerkinbekova, S. Kalybekkyzy, Z. Bakenov, A. Mentbayeva, *J. Alloys Compd.* **2021**, *882*, 160774.
[7] M. Bianchini, M. Roca-Ayats, P. Hartmann, T. Brezesinski, J. Janek, *Angew. Chem.* **2019**, *131*, 10542–10569; *Angew. Chem. Int. Ed.* **2019**, *58*, 10434–10458.
[8] S. Tan, Y. J. Ji, Z. R. Zhang, Y. Yang, *ChemPhysChem* **2014**, *15*, 1956–1969.
[9] T. Zhang, E. Paillard, *Front. Chem. Sci. Eng.* **2018**, *12*, 577–591.
[10] K. Guo, S. Qi, H. Wang, J. Huang, M. Wu, Y. Yang, X. Li, Y. Ren, J. Ma, *Small Sci.* **2022**, *2*, 2100107.
[11] E. Björklund, M. Göttlinger, K. Edström, R. Younesi, D. Brandell, *Batteries & Supercaps* **2020**, *3*, 201–207.
[12] T. Zhang, W. Porcher, E. Paillard, *J. Power Sources* **2018**, *395*, 212–220.
[13] P. Hu, J. Chai, Y. Duan, Z. Liu, G. Cui, L. Chen, *J. Mater. Chem. A* **2016**, *4*, 10070–10083.
[14] X. Cao, X. He, J. Wang, H. Liu, S. Röser, B. R. Rad, M. Evertz, B. Streipert, J. Li, R. Wagner, M. Winter, I. Cekic-Laskovic, *ACS Appl. Mater. Interfaces* **2016**, *8*, 25971–25978.
[15] M. He, L. Hu, Z. Xue, C. C. Su, P. Redfern, L. A. Curtiss, B. Polzin, A. von Cresce, K. Xu, Z. Zhang, *J. Electrochem. Soc.* **2015**, *162*, A1725–A1729.
[16] H. Cai, H. Jing, X. Zhang, M. Shen, Q. Wang, *J. Electrochem. Soc.* **2017**, *164*, A714–A720.
[17] J. Alvarado, M. A. Schroeder, M. Zhang, O. Borodin, E. Gobrogge, M. Olguin, M. S. Ding, M. Gobet, S. Greenbaum, Y. S. Meng, K. Xu, *Mat. Today* **2018**, *21*, 341–353.
[18] K. Hirata, Y. Morita, T. Kawase, Y. Sumida, *J. Power Sources* **2018**, *395*, 163–170.
[19] K. Hirata, Y. Morita, T. Kawase, Y. Sumida, *J. Electrochem. Soc.* **2020**, *167*, 110553.
[20] S. Li, Y. Xue, X. Cui, S. Geng, Y. Huang, *Ionics* **2016**, *22*, 797–801.
[21] X. Cui, H. Zhang, S. Li, Y. Zhao, L. Mao, W. Zhao, Y. Li, X. Ye, *J. Power Sources* **2013**, *240*, 476–485.
[22] C. Li, Y. Chen, Y. Chen, B. Lao, L. Qi, H. Wang, *J. Alloys Compd.* **2019**, *773*, 105–111.
[23] C. Li, Y. Zhao, H. Zhang, J. Liu, J. Jing, X. Cui, S. Li, *Electrochim. Acta* **2013**, *104*, 134–139.
[24] T. Zhang, I. de Meatza, X. Qi, E. Paillard, *J. Power Sources* **2017**, *356*, 97–102.
[25] M. Kerner, N. Plylahan, J. Scheers, P. Johansson, *RSC Adv.* **2016**, *6*, 23327–23334.
[26] S. J. Kang, K. Park, S. H. Park, H. Lee, *Electrochim. Acta* **2018**, *259*, 949–954.
[27] Y. Yamada, J. Wang, S. Ko, E. Watanabe, A. Yamada, *Nat. Energy* **2019**, *4*, 269–280.
[28] A. Mathew, M. J. Lacey, D. Brandell, *J. Power Sources* **2021**, *11*, 100071.
[29] M. J. Lacey, *ChemElectroChem* **2017**, *4*, 1997–2004.
[30] D. J. Xiong, R. Petibon, L. Madec, D. S. Hall, J. R. Dahn, *J. Electrochem. Soc.* **2016**, *163*, A1678–A1685.
[31] B. Gyenes, D. A. Stevens, V. L. Chevrier, J. R. Dahn, *J. Electrochem. Soc.* **2015**, *162*, A278–A283.
[32] M. Genovese, A. J. Louli, R. Weber, C. Martin, T. Taskovic, J. R. Dahn, *J. Electrochem. Soc.* **2019**, *166*, A3342–A3347.
[33] J. Li, L. E. Downie, L. Ma, W. Qiu, J. R. Dahn, *J. Electrochem. Soc.* **2015**, *162*, A1401–A1408.
[34] L. R. Painter, E. T. Arakawa, M. W. Williams, J. C. Ashley, *Radiat. Res.* **1980**, *83*, 1–18.
[35] Y. Wang, S. Nakamura, M. Ue, P. B. Balbuena, *J. Am. Chem. Soc.* **2001**, *123*, 11708–11718.
[36] K. Ciocek, S. Malmgren, M. Hahlin, H. Rensmo, P. Johansson, *J. Phys. Chem. C* **2013**, *117*, 23476–23486.
[37] V. Sharova, A. Moretti, T. Diemant, A. Varzi, R. J. Behm, S. Passerini, *J. Power Sources* **2018**, *375*, 43–52.
[38] Q. Zheng, G. Li, X. Zheng, L. Xing, K. Xu, W. Li, *Energy Environ. Mater.* **2022**, *5*, 906–911.

Research Article
doi.org/10.1002/batt.202200565

[39] E. Björklund, D. Brandell, M. Hahlin, K. Edström, R. Younesi, *J. Electrochem. Soc.* **2017**, *164*, A3054–A3059.
[40] Q. Zhang, J. Pan, P. Lu, Z. Liu, M. W. Verbrugge, B. W. Sheldon, Y. T. Cheng, Y. Qi, X. Xiao, *Nano Lett.* **2016**, *16*, 2011–2016.
[41] H. Bryngelsson, M. Stjerndahl, T. Gustafsson, K. Edström, *J. Power Sources* **2007**, *174*, 970–975.
[42] S. Yang, Y. Zhang, Z. Li, N. Takenaka, Y. Liu, H. Zou, W. Chen, M. Du, X. J. Hong, R. Shang, E. Nakamura, Y. P. Cai, Y. Q. Lan, Q. Zheng, Y. Yamada, A. Yamada, *ACS Energy Lett.* **2021**, *6*, 1811–1820.
[43] J. Xia, J. Self, L. Ma, J. R. Dahn, *J. Electrochem. Soc.* **2015**, *162*, A1424–A1431.

Manuscript received: December 24, 2022
Revised manuscript received: March 1, 2023
Accepted manuscript online: March 2, 2023
Version of record online: March 23, 2023